ELEMENTA
Science of the Anthropocene

Sun, L, et al. 2021. Visible-light-induced peroxymonosulfate activation over $ZnFe_2O_4$ fine nanoparticles for ofloxacin degradation. *Elem Sci Anth*, 9: 1. DOI: https://doi.org/10.1525/elementa.2020.00096

RESEARCH ARTICLE

Visible-light-induced peroxymonosulfate activation over $ZnFe_2O_4$ fine nanoparticles for ofloxacin degradation

Lei Sun[1,2], Gang Cao[1,2], Musheng Xu[1], Gong Cheng[2], Dongsheng Xia[1,2,*], Xiangjuan Yuan[1], and Juan Liu[3,*]

Widespread overuse and misuse of antibiotics has led to unintended consequences, and it is necessary to find effective ways to remove antibiotics. In this study, a visible-light-response photocatalyst zinc ferrite ($ZnFe_2O_4$) was synthesized via a hydrothermal method. Meanwhile, the X-ray diffraction, Brunauer–Emmett–Teller, scanning electron microscope, X-ray photoelectron spectroscopy, and Fourier transform infrared spectra analysis were applied to characterize the structure, morphology, and physicochemical properties of the $ZnFe_2O_4$. The results indicated that the $ZnFe_2O_4$ was circular granular morphology with a particle size of approximately 30–50 nm and the noticeable intergranular agglomeration. The specific surface area, pore volume, and pore diameter of the $ZnFe_2O_4$ were determined to be 126.8655 m^2/g, 0.2046 cm^3/g, and 64.5190 Å, respectively, representing that the $ZnFe_2O_4$ had a large specific surface area. Moreover, the enhancement of degradation efficiency of ofloxacin (OFL) by peroxymonosulfate (PMS) under the visible light (Vis) was systematically evaluated. The results exhibited that the $ZnFe_2O_4$ achieved the relatively optimum catalytic activity with 80.9% of OFL degradation efficiency in 30 min at pH 6.0 under the PMS concentration of 100 mg/L and the corresponding pseudo-first-order kinetic constant of OFL degradation was 0.0438 min^{-1}. In addition, the effects of $ZnFe_2O_4$ dosage, PMS concentration, initial OFL concentration, solution pH, and water matrix on the OFL degradation were comprehensively investigated in the Vis/PMS/$ZnFe_2O_4$ process. Furthermore, the $ZnFe_2O_4$ exhibited excellent stability and reusability for OFL degradation. The Vis/PMS/$ZnFe_2O_4$ process would be a reliable alternative for the degradation of OFL-like antibiotics to solve the increasingly serious problem of antibiotic pollution.

Keywords: $ZnFe_2O_4$, Ofloxacin, Peroxymonosulfate, Photocatalysis

1. Introduction

Antibiotics are often detected in surface water, groundwater, and various sediments due to their widespread usage all over the world (Li et al., 2020a). The presence of antibiotics with low degradability and concentration in the environment, particularly the entire urban water cycle and food chain, poses a serious public health problem (Christou et al., 2017; Liu et al., 2019; Girijan et al., 2020). In addition, contaminants in the soils are partly mobile and easily get into the air or water, becoming a secondary pollutant via natural/uncontrollable process typical of leaching and weathering (Wang et al., 2021). Ofloxacin (OFL) is a typical fluoroquinolone antibiotic administered to both humans and animals, and after administration, approximately 78% of OFL is excreted (Tong et al., 2011). As the biodegradation of OFL is difficult, sewage treatment plants (STPs) have a low removal rate, and the OFL concentrations in the STP effluents of Beijing, Hangzhou, and Vancouver have been determined to be between 0.6 and 1405 ng/L (Xiao et al., 2008; Tong et al., 2011).

Generally, the advanced oxidation processes (AOPs), such as the Fenton or Fenton-like reaction, ozonation or catalytic ozonation, photocatalytic oxidation, electrochemical oxidation, and ionizing radiation, have been widely used for antibiotics degradation in recent years (Anjali and Shanthakumar, 2019; Liu et al., 2020b; Wang and Zhuan, 2020). Moreover, peroxymonosulfate (PMS), the latest in situ chemical oxidation oxidant, has been receiving widespread attentions due to its numerous advantages

[1] Engineering Research Center for Clean Production of Textile Dyeing and Printing, Ministry of Education, Wuhan Textile University, Wuhan, Hubei, China

[2] Environmental Engineering Centre, Shenzhen Academy of Environmental Sciences, Shenzhen, China

[3] Key Laboratory of Water Quality and Conservation in the Pearl River Delta, Ministry of Education, Guangdong Provincial Key Laboratory of Radionuclides Pollution Control and Resources, School of Environmental Science and Engineering, Guangzhou University, Guangzhou, China

* Corresponding authors:
Emails: dongsheng_xia@wtu.edu.cn (Dongsheng Xia); liujuan858585@163.com (Juan Liu)

including safety, stability, and relatively high redox potential of the corresponding intermediate sulfate radicals ($SO_4\bullet^-$) with a long lifetime and strong oxidizing ability (Hu and Long, 2016). Moreover, PMS can be readily activated by heat, ultraviolet (UV) light, alkaline materials, ultrasound, and appropriate transition metal ions (Fe^{2+}, Co^{2+}, and Mn^{2+}; Zhu et al., 2016).

The AOPs involving the production of $SO_4\bullet^-$ by the activation of persulfate have been widely exploited for the degradation of organic pollutants in water (Wacławek et al., 2017). Under normal conditions, the degradation effect of persulfate on organic matter is insignificant; however, under certain conditions after activation, more $SO_4\bullet^-$ with strong oxidizing activity can be produced. Compared with the hydroxyl radical ($\bullet$OH), the $SO_4\bullet^-$ with a higher standard reduction potential (2.5–3.1 V) would be more selective toward target pollutants and require relatively moderate reaction conditions and exhibit a stronger mineralization ability (Yin et al., 2018; Yao et al., 2021).

The nano zinc ferrite (nano-$ZnFe_2O_4$) is a spinel-structured material with good magnetic and catalytic properties, which has been commonly used in the fields of catalysis, magnetic fluid research, and magnetic photocatalysis (Tang et al., 2013). Once the nano-$ZnFe_2O_4$ absorbs photons, the electrons in its valence band become excited and jump to the conduction band. Moreover, the valence band forms strong oxidizing holes, which can oxidize the organic matter at the interface, as well as other substances, through stationary adsorption under the action of diffusion; otherwise, the holes could continue to exert an oxidation-induced electron-transfer effect (Cai et al., 2016).

Photocatalysis, which occurs under exposure to UV light, is also a common method for the environmental pollutant elimination (Ahmed et al., 2014). The conventional photocatalysis utilizes mostly UV from sunlight, which accounts for only 4% of the solar energy. However, through the introduction of catalysts, the utilization rate of sunlight can be effectively improved. The $ZnFe_2O_4$ semiconductor possesses a relatively narrow bandgap of 1.9 eV; thus, its electrons can be excited by visible light (Vis) without any modification (Yao et al., 2014). However, the $ZnFe_2O_4$ exhibited the low pollutant degradation efficiency due to the rapid recombination of photoinduced electron–hole pairs (Fan et al., 2012). To overcome the low-efficiency problem of the photocatalysis, the development of a more efficient catalyst system that would effectively improve the catalytic oxidation efficiency and overcome the existing limitations is important.

The catalytic activity of the catalyst can be effectively improved by modulating its surface area, preparation method, and changing its properties and structures (Wang et al., 2014; Ren et al., 2015; Mady et al., 2019; Zhu et al., 2020). Meanwhile, the preparation of the $ZnFe_2O_4$ catalyst by using the hydrothermal method for PMS activation under Vis has not yet been systematically investigated. Therefore, in this study, the parameters of the catalytic system for the PMS process were regulated, with OFL serving as the representative pollutant, PMS as the oxidant, and $ZnFe_2O_4$ as the catalyst. The $ZnFe_2O_4$ catalyst was synthesized using a hydrothermal method. Under visible-light exposure, the key steps and rates of the catalytic process were investigated with varying catalyst dosage, pollutant concentration, and reaction factors, such as pH, to explore the catalytic activity and degradation mechanism. We believe that the findings of this study will provide technical and valuable insights for the degradation of trace contaminants in wastewater.

2. Materials and method

2.1. Experimental materials

OFL (>98%) was purchased from TCI Chemicals (Tokyo, Japan). Other chemicals such as iron(III) nitrate nonahydrate [$Fe(NO_3)_3{\cdot}9H_2O$], potassium chloride [KCl], sodium carbonate [Na_2CO_3], sodium bicarbonate [$NaHCO_3$], zinc nitrate [$Zn(NO_3)_2{\cdot}6H_2O$], sodium hydroxide [NaOH], hydrogen chloride [HCl], and cetyl trimethyl ammonium bromid [CTAB] were supplied by Sinopharm Chemical Reagent Co., Ltd (Shanghai, China). The PMS and potassium nitrate (KNO_3) were received from Sigma-Aldrich (St. Louis, USA). The High Performance Liquid Chromatography (HPLC) grade acetonitrile (ACN) as the mobile phase was purchased from Fisher Scientific (Oregon, USA). All reagents were of analytical grade and used without any further purification. Ultrapure water (>18.2 MΩ cm), used for all the experimental solutions, was produced from a Milli-Q system (Burlington, USA).

2.2. Synthesis of $ZnFe_2O_4$

Zn $(NO_3)_2{\cdot}6H_2O$ (2.082 g) was dissolved in 35 mL of deionized water in a 250 mL beaker, after which 1 g of CTAB was added as a dispersant to form a uniform solution (Solution A). Thereafter, 5.656 g of Fe $(NO_3)_3{\cdot}9H_2O$ was completely dissolved in 35 mL of deionized water to afford Solution B; Solution B was added to Solution A to yield Solution C. Solution C was placed in a supersonic machine and mixed for 30 min at 25 °C. An NaOH solution (8 M) was added to Solution C dropwise to achieve a pH of 12.24. The resulting solution was subjected to ultrasonic stirring in the water bath (30 °C) for 30 min, after which it was transferred to an autoclave and maintained at 130 °C for 24 h. After the reactor was naturally cooled to room temperature, the precipitate was centrifuged and washed with deionized water to a neutral pH of approximately 6.0–7.0. Subsequently, the resultant was dried in a vacuum oven at 60 °C for 24 h and ground to afford the $ZnFe_2O_4$. The molar ratio among the constituents of the prepared $ZnFe_2O_4$ was Fe:Zn:CTAB = 0.014:0.007:0.0027.

2.3. $ZnFe_2O_4$ characterization

The specific surface area and microstructure of the samples were tested and analyzed using the Micromeritics ASAP 2010 porosimeter (Norcross, USA). The phase composition and microstructure of the $ZnFe_2O_4$ were studied by the PANalytical Empyrean X-ray powder diffraction (XRD) characterization (Etten Leur, the Netherlands) (Liu

et al., 2020a, 2021). Hitachi FlexSEM 1000 Scanning electron microscopy (Tokyo, Japan) was employed to characterize the surface morphology of the $ZnFe_2O_4$ (Yin et al., 2021). The composition and chemical property of the $ZnFe_2O_4$ were characterized by Thermo Fisher VG Multilab2000 X-ray photoelectron spectroscopy (XPS; Oregon, USA).

2.4. Photocatalytic experiment of $ZnFe_2O_4$

Certain amounts of the OFL, PMS solutions, and the $ZnFe_2O_4$ were mixed in the reactor, which was placed on a magnetic stirrer at 20 °C. The NaOH or HCl solution (0.1 M) was used to adjust the pH of the reaction. Afterward, a dark adsorption reaction was conducted for 30 min before illumination. The Xenon lamp was turned on to initiate the reaction. At a certain time interval, samples were taken out, quenched with excess $Na_2S_2O_3$, centrifuged at 10,000 rpm, filtered by a 0.45 μm filter, and further determined. The concentration of OFL was measured by Waters e2695 HPLC instrument (Milford, USA) equipped with a Sunfire C18 column (150 mm × 4.6 mm, 5 μm) and the UV–Vis detector set at 294 nm. The mobile phase was a mixture of water and ACN (v: v = 30:70) at a flow rate of 1.0 mL min^{-1}. The total organic carbon (TOC) of the samples was monitored by the Analytikjena multi N/C 3100 (Jena, Germany).

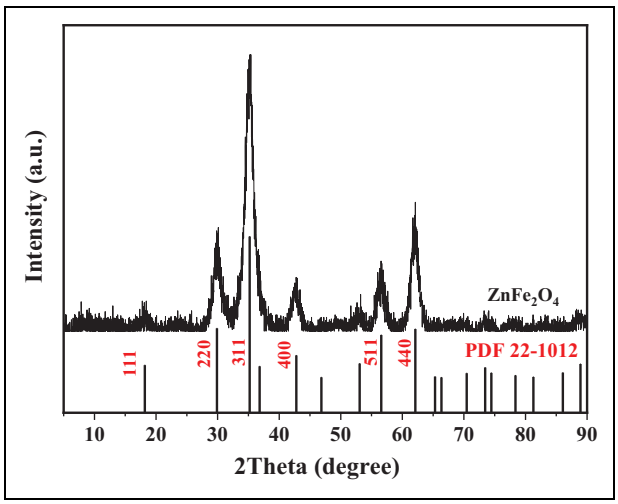

Figure 1. The XRD patterns of $ZnFe_2O_4$. $ZnFe_2O_4$ = zinc ferrite; XRD = X-ray powder diffraction. DOI: https://doi.org/10.1525/elementa.2020.00096.f1

3. Results and discussion

3.1. Characterization of the $ZnFe_2O_4$

The XRD characterization was employed to investigate the crystal structure and chemical composition of $ZnFe_2O_4$ composites, and their diffraction patterns are shown in **Figure 1**. As revealed in **Figure 1**, there were distinct diffraction peaks at 2θ = 18.1°, 29.8°, 35.2°, 42.6°, 56.5°, and 62.0°, which were indexed to (111), (220), (311), (400), (511), and (440) planes (JCPDS card NO.22–1012; Mady et al., 2019). The results indicated that the $ZnFe_2O_4$ exhibited high purity and good crystallinity.

The morphologies of $ZnFe_2O_4$ were observed by SEM and the images were shown in **Figure 2**. It can be observed that the $ZnFe_2O_4$ was circular granular morphology with a particle size of approximately 30–50 nm and the noticeable intergranular agglomeration. This was mainly attributed to the interaction forces among the $ZnFe_2O_4$ particles originating from the magnetic property. Moreover, there also existed some distinct porous structures due to the intergranular agglomeration of the $ZnFe_2O_4$ (**Figure 2**).

The specific surface area and pore structure of the catalyst are important parameters, which could impact the performance of the catalyst, reaction order, and reaction activation energy. The specific surface area, pore volume, and pore diameter of $ZnFe_2O_4$ were determined to be 126.8655 m^2/g, 0.2046 cm^3/g, and 64.5190 Å, respectively, indicating that the $ZnFe_2O_4$ had a large specific surface area. Meanwhile, the N_2 adsorption/desorption isotherm and the pore size distribution of $ZnFe_2O_4$ were displayed in **Figure 3**. The $ZnFe_2O_4$ exhibited N_2 adsorption–desorption isotherms of Type IV, indicating the presence of mesoporous structures with main pore size of 20–50 nm (**Figure 3a** and **b**; Wang et al., 2014). It

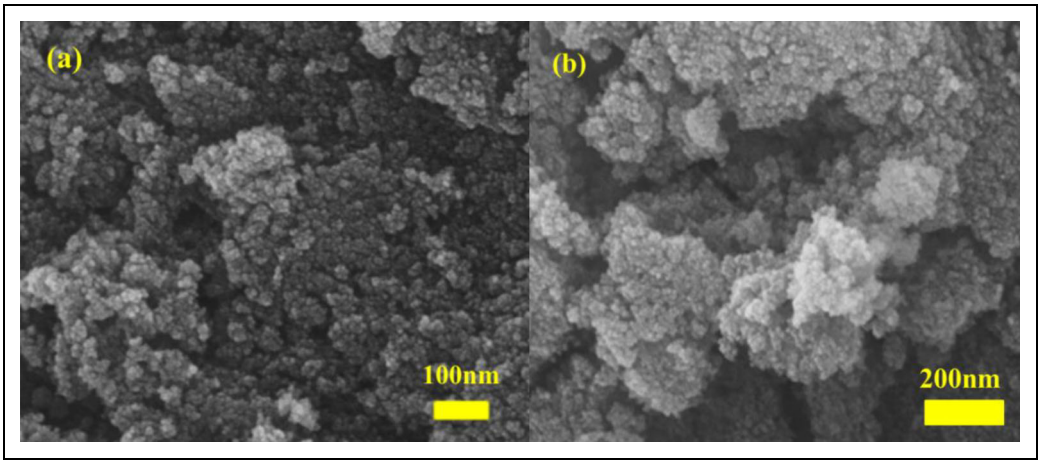

Figure 2. The SEM images of $ZnFe_2O_4$. $ZnFe_2O_4$ = zinc ferrite; SEM = scanning electron microscopy. DOI: https://doi.org/10.1525/elementa.2020.00096.f2

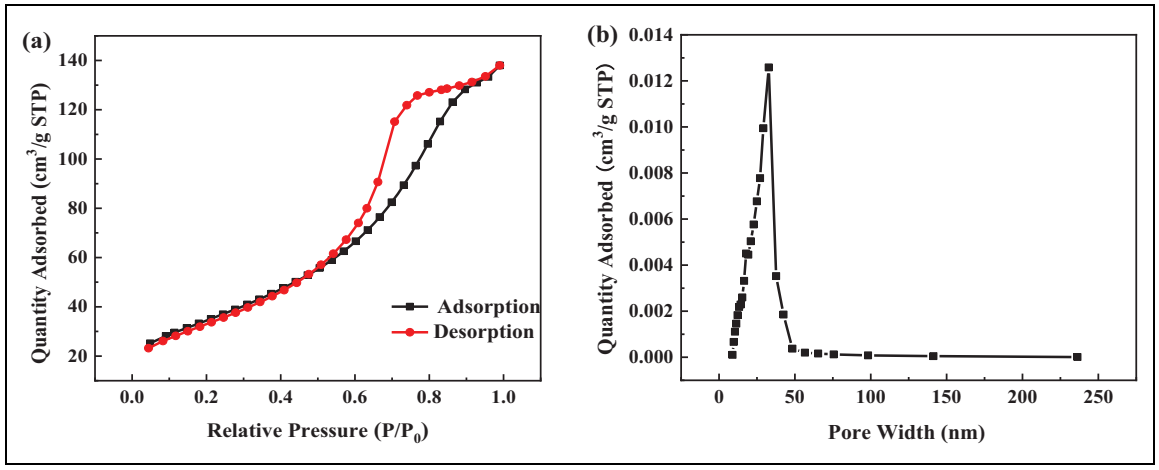

Figure 3. The N_2 adsorption–desorption isotherms (a) and Barrett–Joyner–Halenda pore size distribution plot (b) of $ZnFe_2O_4$. $ZnFe_2O_4$ = zinc ferrite. DOI: https://doi.org/10.1525/elementa.2020.00096.f3

could be speculated that the large specific surface in $ZnFe_2O_4$ would be beneficial for the adsorption, desorption, and diffusion of reactants and products, further greatly accelerating the pollutants degradation (Mady et al., 2019).

The surface element composition and metal state of the $ZnFe_2O_4$ were thoroughly probed through XPS analysis, and the results were illustrated in **Figure 4**. The Fe 2p spectrum exhibited two peaks at around 711.5 and 723.7 eV, which were ascribed to Fe 2p 3/2 and Fe 2p 1/2 in **Figure 4a**, suggesting the presence of Fe^{3+} (Yao et al., 2014; Malakootian et al., 2019; Liu et al., 2020b). The two symmetric peaks at binding energies of 1021.3 and 1045.5 eV shown in **Figure 4b** are assigned to Zn 2p 3/2 and Zn 2p 1/2, suggesting the existence of Zn^{2+} in the $ZnFe_2O_4$ (Yao et al., 2014). The spectrum of O 1s (**Figure 4c**) could be deconvoluted into four peaks with binding energy at 529.18, 529.78, 531.68, and 533.08 eV (Yao et al., 2014). In brief, the peak at 529.18 eV was assigned to the lattice oxygen. The peaks at 529.78 eV and 531.68 eV corresponded to the oxygen-containing functional groups (Mady et al., 2019). The peak at 533.08 eV was assigned to the surface-adsorbed hydroxyl groups (–OH).

3.2. Degradation of OFL in different systems

The OFL degradation efficiencies in different processes including Vis alone, PMS alone, $ZnFe_2O_4$ alone, PMS/$ZnFe_2O_4$, Vis/$ZnFe_2O_4$, Vis/PMS, and Vis/PMS/$ZnFe_2O_4$ processes were evaluated in **Figure 5**. It is noted from **Figure 5a** that the efficiency of OFL removal by the direct adsorption of $ZnFe_2O_4$ was negligible (<3%). Besides, the OFL was slightly removed (<5%) via Vis alone, PMS alone, Vis/$ZnFe_2O_4$, and Vis/PMS processes. Meanwhile, the OFL removal efficiencies in PMS/$ZnFe_2O_4$ and Vis/PMS/$ZnFe_2O_4$ processes were 54.2% and 86.5% within 60 min, respectively. The pseudo-first-order rate constant (k_{obs}) were 0.0125 and 0.0343 min^{-1} in PMS/$ZnFe_2O_4$ and Vis/PMS/$ZnFe_2O_4$ processes (**Figure 5b**). Evidently, the presence of the $ZnFe_2O_4$ and PMS enhanced the degradation efficiency of OFL under the Vis, and the best OFL degradation performance was obtained in Vis/PMS/$ZnFe_2O_4$ process.

3.3. The factors affecting the catalytic activity of $ZnFe_2O_4$

3.3.1. *$ZnFe_2O_4$ dosage*

Here, the effects of the $ZnFe_2O_4$ dosages (0–1,000 mg/L) on the OFL degradation efficiencies were investigated in this study, and the results were revealed in **Figure 6**. As shown in **Figure 6a**, as the $ZnFe_2O_4$ dosage ranged from 100 mg/L to 750 mg/L, the OFL degradation efficiency increased from 35.4% to 80.9% within 30 min reaction. When the $ZnFe_2O_4$ dosage further increased to 1,000 mg/L, the OFL degradation efficiency decreased to 70.4%. The k_{obs} values corresponding to different $ZnFe_2O_4$ dosages were 0.0014, 0.0141, 0.0208, 0.0390, 0.0438, and 0.0349 min^{-1}, respectively (**Figure 6b**). With the increasement of the $ZnFe_2O_4$ dosage, the degradation of OFL was enhanced simultaneously, probably because more active surface sites for oxidation, further to induce more reactive radical species initiation. While at high dosage (1,000 mg/L), the self-aggregation of $ZnFe_2O_4$ would partially affect the surface reactive sites and inhibit the penetration of Vis into the solution as well (Li et al., 2020b).

3.3.2. PMS dosage

The effects of PMS concentrations on the OFL degradation were studied, and the results were represented in **Figure 7**. It is investigated from **Figure 7a** that the OFL degradation efficiency gradually increased from 24.3% to 88.6% (60 min) with the PMS concentration varied from 25 mg/L to 100 mg/L and decreased to 75.3% when the PMS concentration further raised to 250 mg/L. The catalytic effect on OFL was optimal at the PMS concentration of 100 mg/L. The k_{obs} values of the different PMS concentration from 25 mg/L to 250 mg/L were 0.0054, 0.0193,

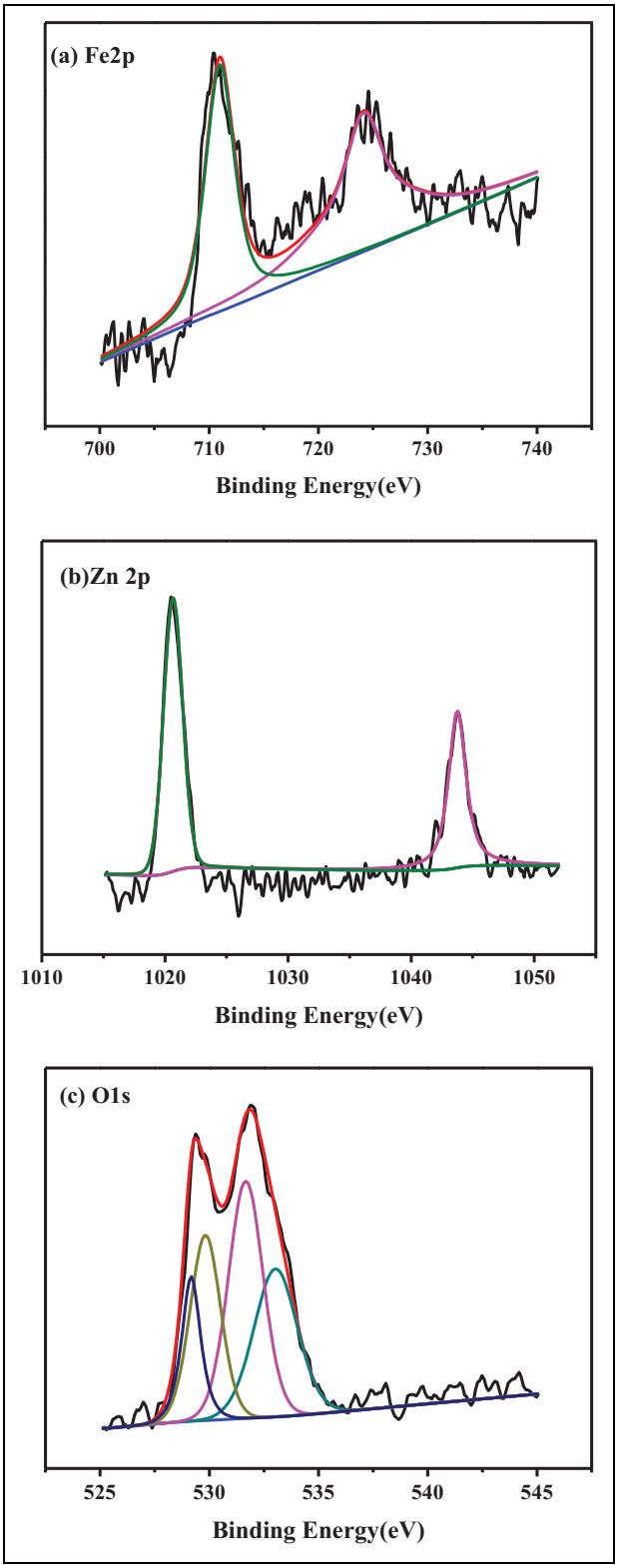

Figure 4. The X-ray photoelectron spectroscopy survey spectra of the $ZnFe_2O_4$. (a) Fe 2p, (b) Zn 2p, and (c) O 1s. $ZnFe_2O_4$ = zinc ferrite. DOI: https://doi.org/10.1525/elementa.2020.00096.f4

0.0438, 0.0334, and 0.0268 min^{-1}, respectively (**Figure 7b**). The excess PMS would act as the scavengers of •OH and SO_4•$^-$, thus leading to the unfavorable consumption of the reactive radicals in the Vis/$ZnFe_2O_4$/PMS process (Zhu et al., 2016). Based on the results, 100 mg/L of PMS was used in subsequent experiments.

3.3.3. OFL concentration

The OFL degradation at initial concentration varying from 2.5 mg/L to 25 mg/L is displayed in **Figure 8a**. The OFL degradation efficiencies during 60 min reaction obviously decreased from 87.5% to 45.5% when the initial OFL concentration rose from 2.5 mg/L to 25 mg/L (**Figure 8a**). More OFL and its intermediates in the aqueous solution could occupy the surface reactive sites of $ZnFe_2O_4$ and also can compete with OFL for the available oxidants in Vis/$ZnFe_2O_4$/PMS system (Li et al., 2020b).

3.3.4. Solution pH

As shown in **Figure 8b**, the effects of solution pH on OFL degradation in Vis/$ZnFe_2O_4$/PMS system were investigated from 3.0 to 9.0. Notably, OFL was rarely removed (less than 5.0%) by direct $ZnFe_2O_4$ adsorption under all the experimental pH conditions (data not shown). When the solution pH varied from 3.0 to 6.0, the Vis/$ZnFe_2O_4$/PMS process achieved an excellent OFL degradation performance and more than 80% of OLF could be removed during 30 min reaction. The k_{obs} values of the OFL degradation were 0.0565, 0.0484, 0.0443, and 0.0438 min^{-1} at the conditions of 3.0, 4.0, 5.0, and 6.0, respectively (**Figure 8b**). The OFL degradation was highly pH-dependent, and the OFL degradation efficiencies were distinctly declined under neutral and alkaline conditions. The k_{obs} value of the OFL degradation was decreasing to 0.0091 min^{-1} at pH 9.0. Thus, it can be seen that the optimal pH value for achieving the maximum catalytic activity of $ZnFe_2O_4$ was 3.0. However, considering the adverse effect of metal–ion dissolution at pH 3.0, the experimental pH value was chosen as 6.0 in the following experiment.

3.3.5. Temperature

Here, the effects of solution temperature (10 °C–40 °C) on the catalytic activity of $ZnFe_2O_4$ were explored, and the results were displayed in **Figure 9a**. As shown in **Figure 9a**, as the temperature increased from 10 °C to 40 °C in the Vis/$ZnFe_2O_4$/PMS process, the k_{obs} constants of OFL degradation were 0.040, 0.0438, 0.0334, and 0.0322 min^{-1}, respectively. The results indicated that the reaction temperature had little impact on the OFL degradation.

3.3.6. Water matrix

Natural organic matter (NOM) and inorganic ions are ubiquitous in surface water, groundwater, and wastewater. The NOM can directly or indirectly react with the reactive radicals and also influence the penetration of the Vis in the Vis/$ZnFe_2O_4$/PMS process. Humic acid (HA) is an important component of NOM. The influences of different water matrix including Cl^- (200 mg/L), NO_3^- (100 mg/L), HCO_3^- (200 mg/L), CO_3^{2-} (200 mg/L), HA (TOC 5 mg/L), and lake water on the OFL degradation were illustrated in **Figure 9b**.

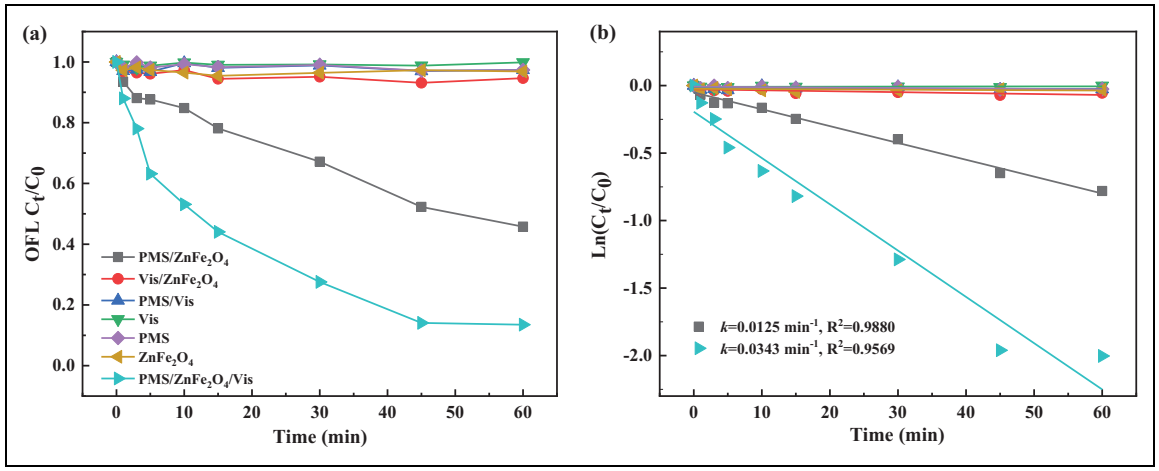

Figure 5. The OFL degradation efficiency (a) and reaction kinetics (b) under different system. Experiment conditions: $ZnFe_2O_4$ = 500 mg/L, OFL concentration = 10 mg/L, PMS concentration = 100 mg/L, pH = 6.0, and T = 20 °C. OFL = ofloxacin; PMS = peroxymonosulfate; $ZnFe_2O_4$ = zinc ferrite. DOI: https://doi.org/10.1525/elementa.2020.00096.f5

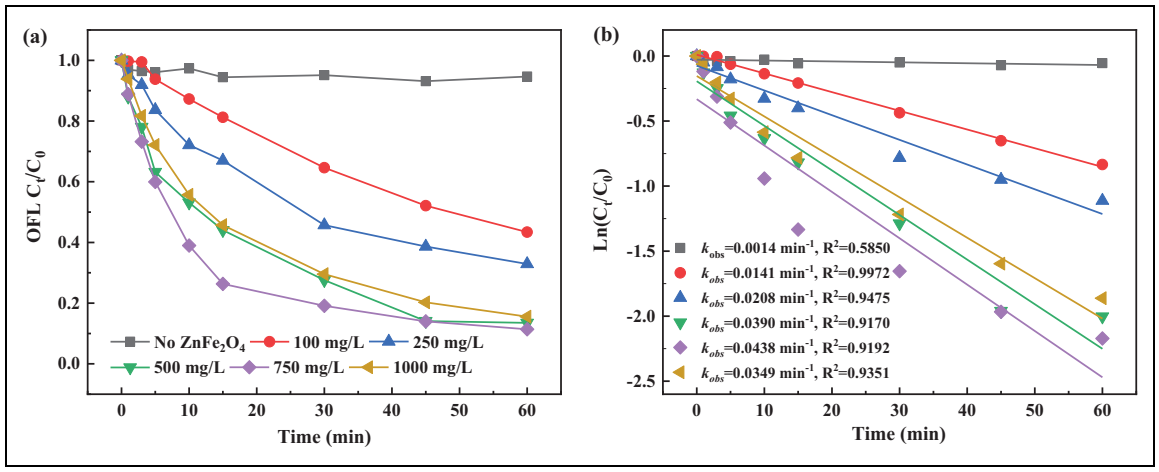

Figure 6. The effects of $ZnFe_2O_4$ dosage (a) and reaction kinetics (b) on the OFL degradation. Experiment conditions: OFL concentration = 10 mg/L, PMS concentration = 100 mg/L, pH = 6.0, and T = 20 °C. $ZnFe_2O_4$ = zinc ferrite; OFL = ofloxacin; PMS = peroxymonosulfate. DOI: https://doi.org/10.1525/elementa.2020.00096.f6

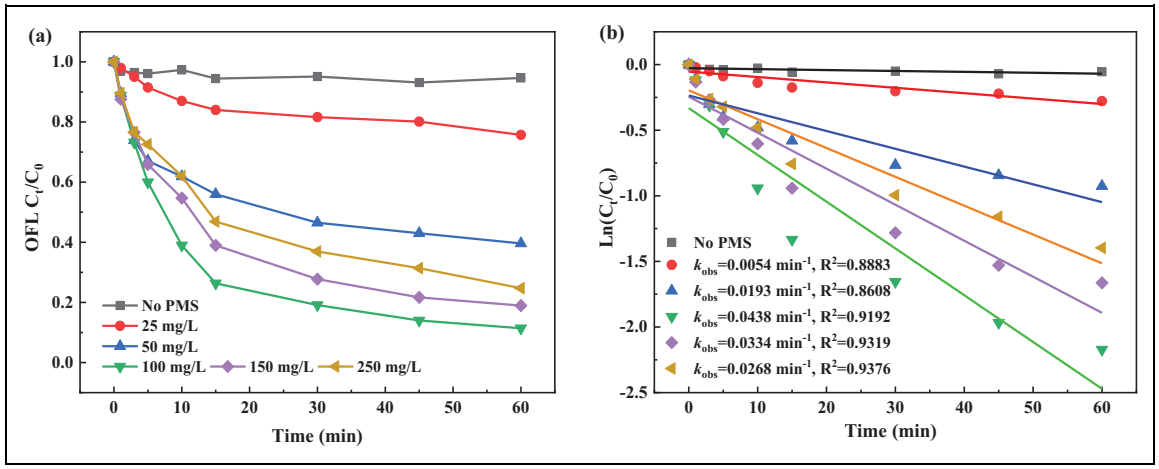

Figure 7. The effects of PMS concentration (a) and reaction kinetics (b) on the OFL degradation. Experiment conditions: $ZnFe_2O_4$ = 750 mg/L, OFL concentration = 10 mg/L, pH = 6.0, and T = 20 °C. PMS = peroxymonosulfate; OFL = ofloxacin; $ZnFe_2O_4$ = zinc ferrite. DOI: https://doi.org/10.1525/elementa.2020.00096.f7

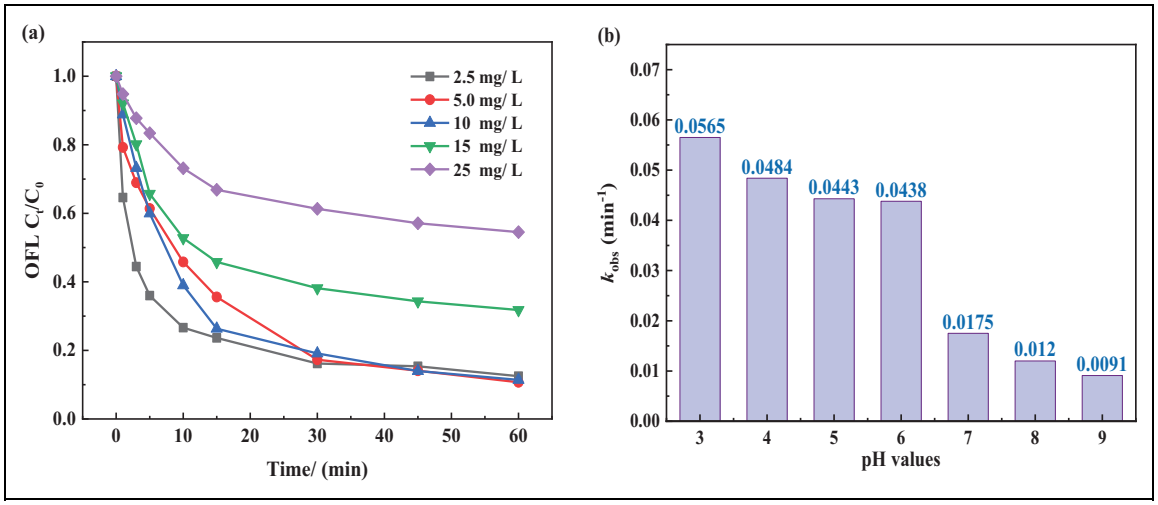

Figure 8. The effects of OFL concentration (a) and pH (b) on the OFL degradation. Experiment conditions: $ZnFe_2O_4$ = 750 mg/L; OFL concentration = 10 mg/L, except for (a); PMS concentration = 100 mg/L; pH = 6.0, except for (b); and T = 20 °C. OFL = ofloxacin; $ZnFe_2O_4$ = zinc ferrite; PMS = peroxymonosulfate. DOI: https://doi.org/10.1525/elementa.2020.00096.f8

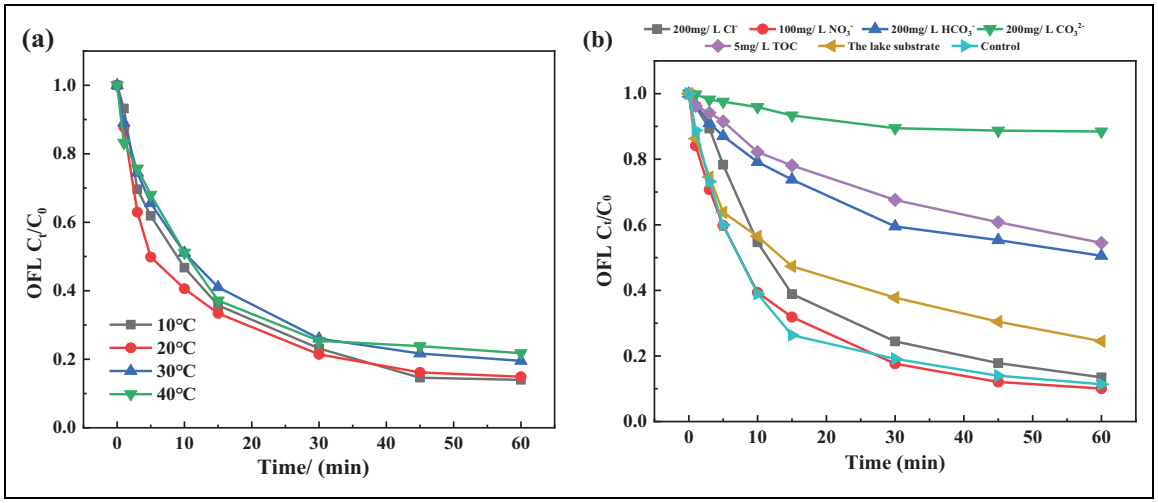

Figure 9. The effects of temperature (a) and water matrix (b) on the OFL degradation. Experiment conditions: $ZnFe_2O_4$ = 750 mg/L; OFL concentration = 10 mg/L; PMS concentration = 100 mg/L; pH = 6.0; and T = 20 °C, except for (a). OFL = ofloxacin; $ZnFe_2O_4$ = zinc ferrite; PMS = peroxymonosulfate. DOI: https://doi.org/10.1525/elementa.2020.00096.f9

There were no obvious effects on the OFL degradation by the inorganic ions (such as Cl^- and NO_3^-) at ambient concentrations, while the presence of CO_3^{2-} and HCO_3^- greatly inhibited the OFL degradation in the Vis/$ZnFe_2O_4$/PMS process. The introduction of CO_3^{2-} affected most obviously on the OFL degradation due to its strong capability for scavenging •OH and SO_4•$^-$ and then formed carbonate radical (CO_3•$^-$), which was more selective and less oxidizing than •OH and SO_4•$^-$. Moreover, the degradation of OFL in Vis/$ZnFe_2O_4$/PMS process was significantly inhibited by HA (TOC was 5 mg/L) and lake water (**Figure 9b**). Note that there were various complex matrix materials coexisting with relatively high concentrations in the surface water. These matrix compounds could compete with OFL for the available oxidants (PMS, •OH, and SO_4•$^-$), thus considerably affecting the OFL degradation, for example, the rate constants for the reactions of NOM with •OH and SO_4•$^-$ were reported to be 1.4 × 10^4 and 6.8 × 10^3 (mgC L^{-1})$^{-1}$ s^{-1}, respectively (Lutze et al., 2015).

3.4. $ZnFe_2O_4$ photocatalytic cycle experiment

To further understand the catalyst activity and the value of reuse, the photocatalytic cyclic experiments of $ZnFe_2O_4$ were conducted. The recovered $ZnFe_2O_4$ was centrifuged

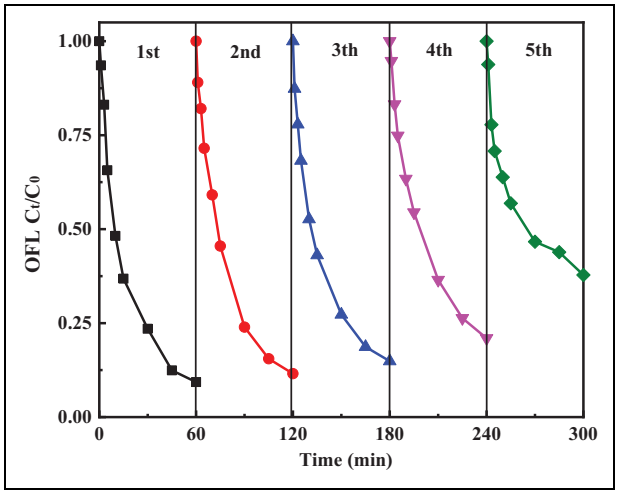

Figure 10. The recycling experiments of $ZnFe_2O_4$. Experimental conditions: $ZnFe_2O_4$ = 750 mg/L, PMS concentration = 100 mg/L, pH = 6, OFL = 10 mg/L, and T = 20 °C. DOI: https://doi.org/10.1525/elementa.2020.00096.f10

and dried at 60°C for 24 h in the recycling experiment and then reused for a subsequent run. As depicted in **Figure 10**, there was no distinct loss of catalytic properties after the third run, and still 62.2% of the OFL could be removed during the fifth cycling experiment in the Vis/$ZnFe_2O_4$/PMS process. The $ZnFe_2O_4$ represented good stability and reusability, which showed a good application potential.

4. Conclusions

In conclusion, the physicochemical properties and the photocatalytic performance of $ZnFe_2O_4$ for OFL degradation were systematically investigated in this study. About 80.9% of OFL removal efficiency within 30 min was achieved in the Vis/$ZnFe_2O_4$/PMS process, and the corresponding k_{obs} constant of OFL degradation was 0.0438 min^{-1}. The characterization results of $ZnFe_2O_4$ on physicochemical properties exhibited that the excellent photocatalytic performance of $ZnFe_2O_4$ was probably attributed to the high specific surface area, pore volume, the abundant functional groups of the surface, and possibly reactive radicals generation. Furthermore, the $ZnFe_2O_4$ represented great reusability and stability in the photocatalytic process. This study may propose a new idea to design an efficient $ZnFe_2O_4$ catalyst for organic pollutants removal.

Data accessibility statement

The data used in this study are available at Visible-light-induced peroxymonosulfate activation over $ZnFe_2O_4$ fine nanoparticles for ofloxacin degradation.opju. https://doi.org/10.6084/m9.figshare.14397635.

Funding

This study was financially supported by the Central Government Guidance for Local Science and Technology Development Projects for Hubei (2018ZYYD024, 2019ZYYD068), the National Natural Science Foundation of China (51808412), and the Knowledge Innovation Program of Shenzhen (JCYJ20160526162154729).

Competing interests

The authors declare that they have no conflict of interest.

Author contributions

Contributed to the conception and design: LS, XY.
Contributed to the acquisition of data: GC, MX.
Contributed to the analysis and interpretation of data: GC.
Drafted and/or revised the article: JL.
Approved the submitted version for publication: DX.

References

Ahmed, MM, Brienza, M, Goetz, V, Chiron, S. 2014. Solar photo-Fenton using peroxymonosulfate for organic micropollutants removal from domestic wastewater: Comparison with heterogeneous TiO_2 photocatalysis. *Chemosphere* **117**: 256–261. DOI: http://dx.doi.org/10.1016/j.chemosphere.2014.07.046.

Anjali, R, Shanthakumar, S. 2019. Insights on the current status of occurrence and removal of antibiotics in wastewater by advanced oxidation processes. *Journal of Environmental Management* **246**: 51–62. DOI: http://dx.doi.org/10.1016/j.jenvman.2019.05.090.

Cai, C, Zhang, Z, Liu, J, Shan, N, Zhang, H, Dionysiou, DD. 2016. Visible light-assisted heterogeneous Fenton with $ZnFe_2O_4$ for the degradation of Orange II in water. *Applied Catalysis B: Environmental* **182**: 456–468. DOI: http://dx.doi.org/10.1016/j.apcatb.2015.09.056.

Christou, A, Agüera, A, Bayona, JM, Cytryn, E, Fotopoulos, V, Lambropoulou, D, Manaia, CM, Michael, C, Revitt, M, Schröder, P, Fatta-Kassinos, D. 2017. The potential implications of reclaimed wastewater reuse for irrigation on the agricultural environment: The knowns and unknowns of the fate of antibiotics and antibiotic resistant bacteria and resistance genes—A review. *Water Research* **123**: 448–467. DOI: http://dx.doi.org/10.1016/j.watres.2017.07.004.

Fan, G, Tong, J, Li, F. 2012. Visible-light-induced photocatalyst based on cobalt-doped zinc ferrite nanocrystals. *Industrial & Engineering Chemistry Research* **51**(42): 13639–13647. DOI: http://dx.doi.org/10.1021/ie201933g.

Girijan, SK, Paul, R, VJ, RK, Pillai, D. 2020. Investigating the impact of hospital antibiotic usage on aquatic environment and aquaculture systems: A molecular study of quinolone resistance in *Escherichia coli*. *Science of the Total Environment* **748**: 141538. DOI: http://dx.doi.org/10.1016/j.scitotenv.2020.141538.

Hu, P, Long, M. 2016. Cobalt-catalyzed sulfate radical-based advanced oxidation: A review on heterogeneous catalysts and applications. *Applied Catalysis B: Environmental* **181**: 103–117. DOI: http://dx.doi.org/10.1016/j.apcatb.2015.07.024.

Li, F, Chen, L, Bao, Y, Zheng, Y, Huang, B, Mu, Q, Feng, C, Wen, D. 2020a. Identification of the priority antibiotics based on their detection frequency, concentration, and ecological risk in urbanized coastal water. *Science of the Total Environment* **747**: 141275. DOI: http://dx.doi.org/10.1016/j.scitotenv.2020.141275.

Li, L, Niu, CG, Guo, H, Wang, J, Ruan, M, Zhang, L, Liang, C, Liu, HY, Yang, YY. 2020b. Efficient degradation of Levofloxacin with magnetically separable $ZnFe_2O_4$/NCDs/Ag_2CO_3 Z-scheme heterojunction photocatalyst: Vis-NIR light response ability and mechanism insight. *Chemical Engineering Journal* **383**. DOI: http://dx.doi.org/10.1016/j.cej.2019.123192.

Liu, J, Li, N, Zhang, WL, Wei, XD, Tsang, DCW, Sun, YB, Luo, XW, Bao, ZA, Zheng, WT, Wang, J, Xu, GL, Hou, LP, Chen, YH, Feng, YX. 2019. Thallium contamination in farmlands and common vegetables in a pyrite mining city and potential health risks. *Environmental Pollution* **248**: 906–915. DOI: http://dx.doi.org/10.1016/j.envpol.2019.02.092.

Liu, J, Ren, S, Cao, J, Tsang, D, Beiyuan, J, Peng, Y, Fang, F, She, J, Yin, M, Shen, N, Wang, J. 2021. Highly efficient removal of thallium in wastewater by MnFe2O4-biochar composite. *Journal of Hazardous Materials* **401**: 123311. DOI: https://doi.org/10.1016/j.jhazmat.2020.123311.

Liu, J, Wei, X, Zhou, Y, Tsang, D, Bao, Z, Yin, M, Lippold, H, Yuan, W, Wang, J, Feng, Y, Chen, D. 2020a. Thallium contamination health risk assessment and source apportionment in common vegetables. *Science of Total Environment* **703**: 135547. DOI: https://doi.org/10.1016/j.scitotenv.2019.135547.

Liu, J, Yin, ML, Xiao, TF, Zhang, CS, Tsang, DCW, Bao, ZA, Zhou, YT, Chen, YH, Luo, XW, Yuan, WH, Wang, J. 2020b. Thallium isotopic fractionation in industrial process of pyrite smelting and environmental implications. *Journal of Hazardous Materials* **384**: 11. DOI: http://dx.doi.org/10.1016/j.jhazmat.2019.121378.

Lutze, HV, Bircher, S, Rapp, I, Kerlin, N, Bakkour, R, Geisler, M, von Sonntag, C, Schmidt, TC. 2015. Degradation of chlorotriazine pesticides by sulfate radicals and the influence of organic matter. *Environmental Science & Technology* **49**(3): 1673–1680. DOI: http://dx.doi.org/10.1021/es503496u.

Mady, AH, Baynosa, ML, Tuma, D, Shim, J-J. 2019. Heterogeneous activation of peroxymonosulfate by a novel magnetic 3D gamma-MnO_2@$ZnFe_2O_4$/rGO nanohybrid as a robust catalyst for phenol degradation. *Applied Catalysis B: Environmental* **244**: 946–956. DOI: http://dx.doi.org/10.1016/j.apcatb.2018.11.086.

Malakootian, M, Nasiri, A, Asadipour, A, Kargar, E. 2019. Facile and green synthesis of $ZnFe_2O_4$@CMC as a new magnetic nanophotocatalyst for ciprofloxacin degradation from aqueous media. *Process Safety and Environmental Protection* **129**: 138–151. DOI: http://dx.doi.org/10.1016/j.psep.2019.06.022.

Ren, Y, Lin, L, Ma, J, Yang, J, Feng, J, Fan, Z. 2015. Sulfate radicals induced from peroxymonosulfate by magnetic ferrospinel MFe_2O_4 (M = Co, Cu, Mn, and Zn) as heterogeneous catalysts in the water. *Applied Catalysis B: Environmental* **165**: 572–578. DOI: http://dx.doi.org/10.1016/j.apcatb.2014.10.051.

Tang, W, Su, Y, Li, Q, Gao, S, Shang, JK. 2013. Superparamagnetic magnesium ferrite nanoadsorbent for effective arsenic (III, V) removal and easy magnetic separation. *Water Research* **47**(11): 3624–3634. DOI: http://dx.doi.org/10.1016/j.watres.2013.04.023.

Tong, C, Zhuo, X, Guo Y. 2011. Occurrence and risk assessment of four typical fluoroquinolone antibiotics in raw and treated sewage and in receiving waters in Hangzhou, China. *Journal of Agricultural and Food Chemistry* **59**(13): 7303–7309. DOI: http://dx.doi.org/10.1021/jf2013937.

Wacławek, S, Lutze, HV, Grübel, K, Padil, VVT, Černík, M, Dionysiou, DD. 2017. Chemistry of persulfates in water and wastewater treatment: A review. *Chemical Engineering Journal* **330**: 44–62. DOI: http://dx.doi.org/10.1016/j.cej.2017.07.132.

Wang, J, Wang, L, Wang, Y, Tsang, D, Yang, X, Beiyuan, J, Yin, M, Xiao, T, Jiang, Y, Lin, W, Zhou, Y, Liu, J, Wang, L, Zhao, M. 2021. Emerging risks of toxic matal(loid)s in soil-vegetables influenced by steelmaking activities and isotopic source apportionment. *Environment International* **146**: 106207. DOI: https://doi.org/10.1016/j.envint.2020.106207.

Wang, J, Zhuan, R. 2020. Degradation of antibiotics by advanced oxidation processes: An overview. *Science of the Total Environment* **701**. DOI: http://dx.doi.org/10.1016/j.scitotenv.2019.135023.

Wang, Y, Sun, H, Ang, HM, Tade, MO, Wang, S. 2014. Facile synthesis of hierarchically structured magnetic MnO_2/$ZnFe_2O_4$ hybrid materials and their performance in heterogeneous activation of peroxymonosulfate. *ACS Applied Materials & Interfaces* **6**(22): 19914–19923. DOI: http://dx.doi.org/10.1021/am505309b.

Xiao, Y, Chang, H, Jia, A, Hu, J. 2008. Trace analysis of quinolone and fluoroquinolone antibiotics from wastewaters by liquid chromatography–electrospray tandem mass spectrometry. *Journal of Chromatography A* **1214**(1): 100–108. DOI: http://dx.doi.org/10.1016/j.chroma.2008.10.090.

Yao, B, Luo, Z, Zhi, D, Hou, D, Luo, L, Du, S, Zhou, Y. 2021. Current progress in degradation and removal methods of polybrominated diphenyl ethers from water and soil: A review. *Journal of Hazardous Materials* **403**: 123674. DOI: http://dx.doi.org/10.1016/j.jhazmat.2020.123674.

Yao, Y, Cai, Y, Lu, F, Qin, J, Wei, F, Xu, C, Wang, S. 2014. Magnetic $ZnFe_2O_4$-C_3N_4 hybrid for photocatalytic degradation of aqueous organic pollutants by visible light. *Industrial & Engineering Chemistry Research* **53**(44): 17294–17302. DOI: http://dx.doi.org/10.1021/ie503437z.

Yin, M, Zhou, Y, Tsang, D, Beiyuan, J, Song, L, She, J, Wang, J, Zhu, L, Fang, Fa, Wang, L, Liu, Y, Song, G, Chen, D, Xiao, T. 2021. Emergent thallium exposure from uranium mill tailings. *Jounal of Hazardous Materials* **407**: 124402. DOI: https://doi.org/10.1016/j.jhazmat.2020.124402.

Yin, R, Guo, W, Wang, H, Du, J, Zhou, X, Wu, Q, Zheng, H, Chang, J, Ren, N. 2018. Enhanced peroxymonosulfate activation for sulfamethazine degradation by ultrasound irradiation: Performances and mechanisms. *Chemical Engineering Journal* **335**: 145–153. DOI: http://dx.doi.org/10.1016/j.cej.2017.10.063.

Zhu, K, Wang, J, Wang, Y, Jin, C, Ganeshraja, AS. 2016. Visible-light-induced photocatalysis and peroxymonosulfate activation over $ZnFe_2O_4$ fine nanoparticles for degradation of Orange II. *Catalysis Science & Technology* **6**(7): 2296–2304. DOI: http://dx.doi.org/10.1039/c5cy01735a.

Zhu, S, Xu, Y, Zhu, Z, Liu, Z, Wang, W. 2020. Activation of peroxymonosulfate by magnetic Co-Fe/SiO_2 layered catalyst derived from iron sludge for ciprofloxacin degradation. *Chemical Engineering Journal* **384**. DOI: http://dx.doi.org/10.1016/j.cej.2019.123298.

How to cite this article: Sun, L, Cao, G, Xu, M, Cheng, G, Xia, D, Yuan, X, Liu, J. 2021. Visible-light-induced peroxymonosulfate activation over $ZnFe_2O_4$ fine nanoparticles for ofloxacin degradation. *Elementa: Science of Anthropocene* 9(1). DOI: https://doi.org/10.1525/elementa.2020.00096

Domain Editor-in-Chief: Steven Allison, University of California, Irvine, CA, USA

Guest Editor: Chuan-Chou Shen, Department of Geosciences, National Taiwan University, Taipei, Taiwan

Knowledge Domain: Ecology and Earth Systems

Part of an Elementa Special Feature: Pan-Pacific Anthropocene

Published: June 8, 2021 **Accepted:** April 23, 2021 **Submitted:** July 4, 2020

ELEMENTA Science of the Anthropocene

Elem Sci Anth is a peer-reviewed open access journal published by University of California Press.

OPEN ACCESS